

Effects of smart flap on aerodynamic performance of sinusoidal leading-edge wings at low Reynolds numbers

Proc IMechE Part G:
J Aerospace Engineering
2021, Vol. 235(4) 439–450
© © IMechE 2020
Article reuse guidelines:
sagepub.com/journals-permissions
DOI: 10.1177/0954410020946903
journals.sagepub.com/home/pig



AA Mehraban¹, MH Djavareshkian¹ , Y Sayegh¹,
B Forouzi Feshalami¹ , Y Azargoon¹, AH Zaree¹ and
M Hassanalian²

Abstract

Sinusoidal leading-edge wings have shown a high performance after the stall region. In this study, the role of smart flaps in the aerodynamics of smooth and sinusoidal leading-edge wings at low Reynolds numbers of 29,000, 40,000 and 58,000 is investigated. Four wings with NACA 634-021 profile are firstly designed and then manufactured by a 3 D printer. Beam bending equation is used to determine the smart flap chord deflection. Next, wind tunnel tests are carried out to measure the lift and drag forces of proposed wings for a wide range of angles of attack, from zero to 36 degrees. Results show that using trailing-edge smart flap in sinusoidal leading-edge wing delays the stall point compared to the same wing without flap. However, a combination of smooth leading-edge wing and smart flap advances the stall. Furthermore, it is found that wings with smart flap generally have a higher lift to drag ratio due to their excellent performance in producing lift.

Keywords

Biomimetic, experimental aerodynamics, humpback whale, low Reynolds number, sinusoidal leading-edge, smart flap

Date received: 23 February 2020; accepted: 9 July 2020

Introduction

Since nature has developed processes, objects, materials, and functions to increase its efficiency, it has the best answers when we seek to improve or optimize a system. Thus, the fields of biomimetic and bioinspiration allow us to mimic biology or nature to develop methods for increasing the performance of all types of transportations involving land, sea, and air. For example, due to the high maneuverability of humpback whale, many researches have been conducted to reveal secrets behind their excellent swimming performance. Scientists have shown that humpback whales use their sinusoidal leading-edge flippers to increase their agility.¹ Therefore, flippers of humpback whales have been inspired by many scholars to improve the aerodynamic performance of unmanned aerial vehicles (UAVs),^{2,3} aircraft wings,^{4,5} flapping wings,⁶ wind turbine blades,^{7–9} hydrofoils^{10,11} and compressor cascades.¹²

Primary studies were performed to measure aerodynamic forces and visualize the flow field around the wings with sinusoidal leading-edge. By conducting experimental research on NACA 634-021 airfoils at

$Re = 1.83 \times 10^5$, Johari et al.¹³ revealed that the stall angle is delayed by using leading-edge protuberance airfoil. They explained that attachment of flow over the protuberances is the main reason for this characteristic. Results also indicated that the lift coefficient of sinusoidal leading-edge wing is higher than that of a conventional wing in the poststall regime. By measuring pressure distribution and flow velocity, and visualizing the flow field by oil-film method, Zverkov et al.¹⁴ compared the boundary layer structure of wavy and classical wings at $Re = 1.7 \times 10^5$ and zero degree angle of attack (α). They attributed the discrepancy between boundary layer structures of two aforementioned wings to transition position. By conducting an experimental study at $Re = 1.2 \times 10^5$,

¹Department of Mechanical Engineering, Ferdowsi University of Mashhad, Mashhad, Iran

²Department of Mechanical Engineering, New Mexico Tech, Socorro, NM, USA

Corresponding author:

MH Djavareshkian, Department of Mechanical Engineering, Ferdowsi University of Mashhad, Mashhad, Iran.

Email: javareshkian@um.ac.ir

Hansen et al.¹⁵ concluded that reducing the tubercle amplitude results in a higher maximum lift coefficient and larger stall angle. However, in the poststall regime, increased tubercle amplitude is more desirable. Dropkin et al.¹⁶ performed a numerical simulation to visualize the flow pattern around a leading-edge protuberances NACA63 airfoil at $Re = 1.83 \times 10^5$. They stated that lift improvement is because of low-pressure pockets in the troughs that are symmetric and periodic at low angles of attack and stay persists to high angles of attack. To control the flow around a smooth leading-edge airfoil at a low Reynolds number of 50,000, Zhang et al.¹⁷ experimentally investigated the capability of a leading-edge-protuberance technique for a wide range of angles of attack. They indicated that lift and lift to drag ratio of the smooth leading-edge airfoil could be enhanced by 25% and 39.2% using sinusoidal leading-edge, respectively.

More recently, the effects of different flow patterns and geometric parameters have been investigated. Effects of periodic and aperiodic flow patterns on leading-edge protuberance airfoils were studied by Cai et al.¹⁸ In another research, Cai et al.¹⁹ assessed aerodynamic performance of a single leading-edge protuberance NACA63₄-021 airfoil at $Re = 1 \times 10^5$. They demonstrated that the performance of the modified airfoil could be improved in the poststall region while it is declined in the prestall area. Bolzon et al.²⁰ studied the role of a single tubercle at a swept wing's tip in the performance of a NACA0021 wing at $Re = 2.25 \times 10^5$. Aerodynamic forces, as well as flow patterns around a swept tubercle wing, were measured by Bolzon et al.²¹ They clarified that tubercles enhance lift to drag ratio by 3% before the stall region. By conducting numerical simulation on a NACA4415 airfoil, at $Re = 1.2 \times 10^5$, Aftab and Ahmad²² concluded that aerodynamic performance of spherical tubercles evidently outweighs that of sinusoidal tubercles.

Lin et al.²³ numerically studied the effects of trailing-edge protuberances on flow characteristics of a NACA0015 airfoil. They expressed that increment of the amplitude and wavelength of the tubercle enhances the power coefficient by 16.4% in comparison with a straight blade. A leading-edge protuberance NACA0012 wing with interchangeable trailing-edge was tested by Prigent et al.²⁴ to reveal how interchangeable trailing-edge can impact on the wake properties. Rostamzadeh et al.²⁵ numerically aimed at capturing flow patterns around a leading-edge protuberance NACA0021 wing in transitional and near turbulent flow regimes of $Re = 1.2 \times 10^5$ and $Re = 15 \times 10^5$. They stated that in a turbulent flow regime, the conventional wing produces a higher lift force than tubercled foil and shows gradual stall. Guerreiro and Sousa²⁶ tested the effects of low Reynolds numbers of 70,000 and 140,000 on aerodynamic forces and flow characteristics of a leading-

edge protuberance NASALS(1)0417 wing. They showed that the advantages of sinusoidal leading-edge wings are extended to low angles of attack at low Reynolds number flows. Effects of Reynolds number, ranging from 10,000 to 60,000, on the aerodynamics of a NACA0012 wing with leading-edge protuberance were investigated by Yasuda et al.²⁷ They indicated that for $\alpha > 8^\circ$, lift of modified wing increases regardless of Reynolds number variation.

Numerical simulations over finite wings with leading-edge protuberances were conducted by Esmaili et al.²⁸ at a Reynolds number of 140,000. In this study, they compared different turbulence modeling schemes, including RANS and DES, before and after stall regions. Moreover, the capability of the DES approach for an accurate evaluation of flow physics before and after stall was proved. The effects of the spanwise distribution of tubercles on a UAV wing were numerically evaluated by Papadopoulos et al.²⁹ They expressed that higher aerodynamic performance and efficiency could be achieved by adding tubercles. Experimental and numerical studies were conducted by Sreejith and Sathyabhama³⁰ to discover the effects of leading-edge tubercles on a cambered airfoil E216 before stall at a Reynolds number of 100,000. They manifested that tubercles cause laminar separation bubbles formation and flow field to be changed significantly. Recent achievements in the field of sinusoidal leading-edge wings have comprehensively been reviewed in.^{8,31,32}

On the other hand, adaptive airfoils could significantly improve the aerodynamic performance especially during take-off and landing phases where a trailing-edge flap plays an important role.³³ It was found that this type of airfoils has less drag and higher lift and can delay the stall.³⁴ Furthermore, it enhances the maneuverability of air vehicles. It was also indicated that adaptive airfoils can decline the vortex size and its power.³⁵ One way to construct an airfoil with variable geometry is to use smart materials like piezoelectric and shape memory alloy. Smart materials have been of interest as they result in less weight penalty.³⁶ They also have been applied in various engineering applications, such as blades of helicopters,³⁷ spoiler of racecar,³⁸ wind turbine³⁹ and suspended bridge.⁴⁰ One way to derive the varied profile of the airfoil after applying smart materials is to use the cantilever beam equation.⁴¹ The beam bending equation is the same smart flap chord deflection. Therefore, the obtained geometry can be considered as a smart flap. Djavareshkian et al.⁴² numerically showed that since the airfoil with a smart flap is considered as a single element, it undergoes less separation than the airfoil with a conventional flap which is called a double element. In another study, Djavareshkian et al.⁴³ showed that a NACA4412 hydrofoil with a smart flap produces a higher lift to drag ratio compared to the airfoil with conventional

flap. By conducting the three-dimensional numerical simulation, Djvarehshkian and Esmaili³⁸ demonstrated that the pressure coefficient distribution for a wing with a smart flap is smoother than that of a wing with a conventional flap.

In spite of the great effort of research in this area, the effects of flaps on the aerodynamic performance of leading-edge protuberance wings have not been investigated yet. Therefore, the main objective of this research study is to compare the aerodynamic forces between sinusoidal and smooth leading-edge wings with smart flaps to reveal whether this flap type can improve the performance of wavy wings. As flaps play a crucial role in controlling the fluid flow and enhance the performance in different industries,⁴⁴⁻⁴⁶ the findings of this research are applicable. To the authors' knowledge, there are very few researches on this topic in the range of low Reynolds number flow. Therefore, this study is performed in Reynolds numbers of 29,000, 40,000 and 58,000. Low Reynolds number flow is of interest because Micro Air Vehicles (MAVs) or UAVs are widely used in this flow regime.⁴⁷ Moreover, since classical flow control methods including, boundary layer suction⁴⁸ or thermal camber,⁴⁹ are very energy consuming and also lead to weight penalty, sinusoidal leading-edge wings as a way of flow control would be a remarkable achievement. The aim of this paper is to enhance the aerodynamic performances of these wings by using smart flaps. The rest of this paper is organized as follows. In section 2, experimental setups, including wing modeling, wind tunnel characteristics, and measurement instruments, are proposed. Results and discussion are presented in section 3. Finally, a summary and conclusions are shown in Section 4.

Experimental setup

Preparation of wings

The design procedure of the sinusoidal leading-edge wing in the current study is the same as that mentioned by Lohry et al.⁵⁰ As can be seen in Figure 1, three airfoils are used to design the wings. The main airfoil has the profile of the NACA 63₄-021 airfoil. All three airfoils have the same profile (x and y) in 70% of chord from trailing-edge. However, the profile of through and peak airfoils is scaled in the x -direction in 30% of chord from leading-edge. It should be noted that the thickness of all three airfoils is the same in the chordwise direction. This design procedure has also been used in.^{11,51}

The designed and constructed wings used in the experiments are shown in Figure 2. All wings have the NACA 63₄-021 profile with a chord (c) and a span of 10 cm and 29 cm, respectively. They are firstly designed in SolidWorks software and then fabricated by a 3-D printer. All wings were hand polished after

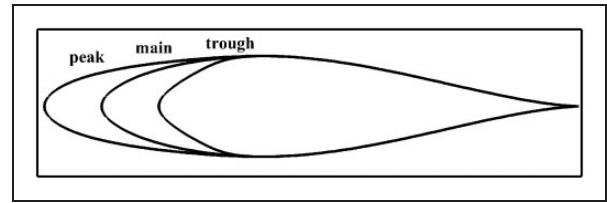


Figure 1. A cross-section of the sinusoidal leading-edge wing.⁵¹

construction and their surface roughness height is much less than the critical roughness height mentioned by Custodio et al.⁵¹ Two wings have smooth leading-edge, which one of them has no flap (A), and the other one uses smart flap (A₁). The other two wings have sinusoidal leading-edge with wavelength and amplitude of $0.5c$ and $0.12c$, respectively. These two wings are named based on their flaps. One that has no flap is named B, and the other one with a smart flap is called B₁. The geometric properties of the four tested wings are summarized in Table 1.

In this study, instead of using smart materials like piezoelectric or shape memory alloy to change the camber of the airfoil, the profile of the smart flap is derived by considering it as a cantilever beam with uniformly varying load (see Figure 3).

The beam bending equation is used to determine the smart flap chord deflection.

$$Y = \frac{\omega_0(-X^5 + 2B^2X^3 - B^4X)}{120EIB}, \quad (1)$$

$$Y_{Midline} = K(-X^5 - a^2X^3 + X)$$

$$a = \frac{1 - B^4}{B^2} \quad (2)$$

where X and Y are horizontal and vertical Cartesian coordinates, respectively. B and I denote the length of the beam (m) and area moment of inertia (m⁴) respectively. Also, E is Young's modulus and ω_0 shows weight/unit length (N/m). The coefficients of Eq. (2) are computed by an iterative process in FORTRAN, and the content of the coefficient is either increased or decreased until the favorable profile is attained. It is worth mentioning that the same profile was also used by Chinnassamy and Chen.⁴¹ In contrast to classic flaps that hinged distinctly to the wing, wings with smart flap maintain a continuous slope in the camber line. This technique results in a higher lift, lower drag and decrease in radar cross-section.³³ The difference between the profiles of the wings with smart flap (wings A₁ and B₁) and those without flap (wings A and B) is shown in Figure 4. It should be noted that the wing and the smart flap are completely rigid, and the flap is not hinged to the wing. That is to say, the wing and the flap are an integral part, and the geometry does not change

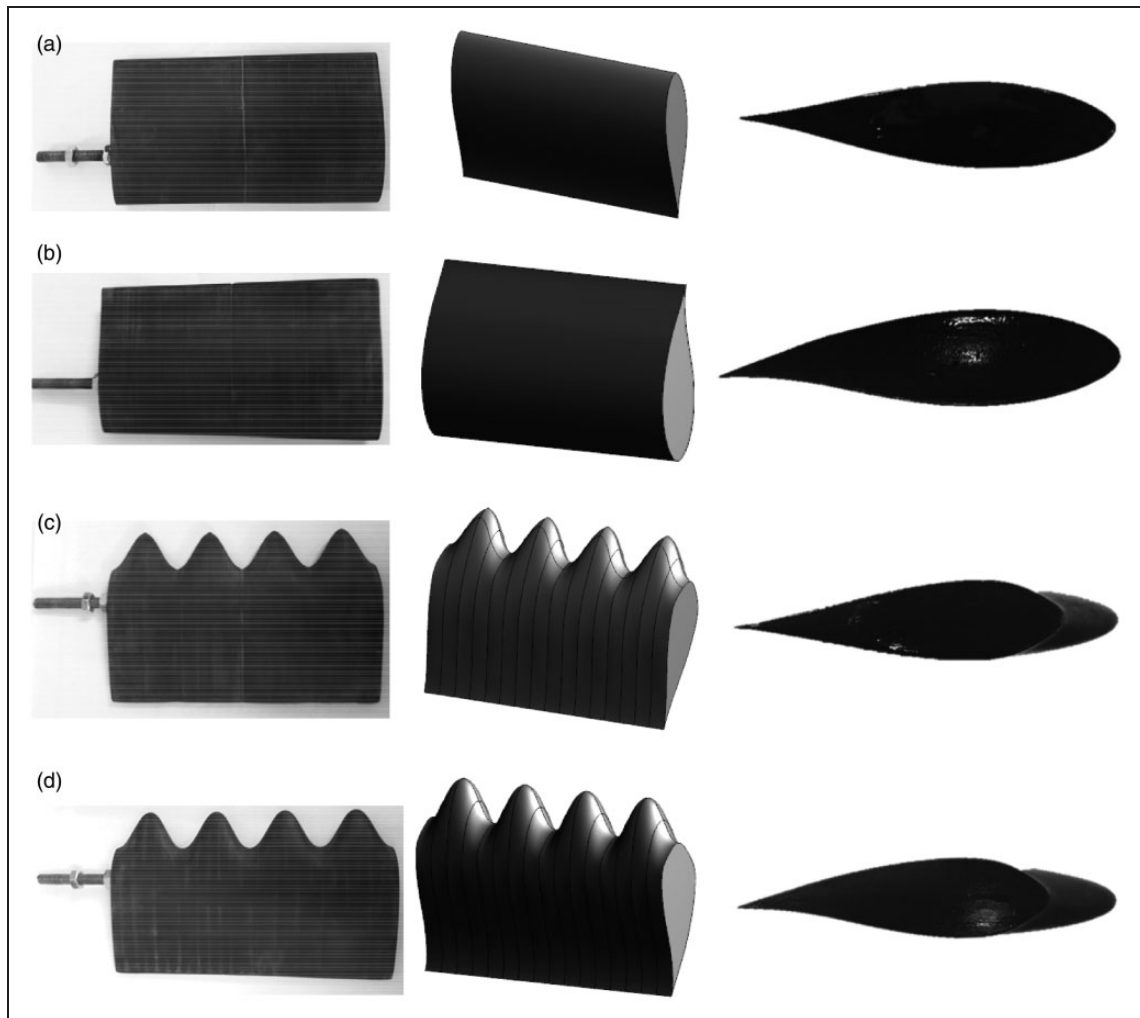


Figure 2. Designed and prototyped wings: (a) wing A (smooth leading-edge wing without flap), (b) wing A₁ (smooth leading-edge wing with smart flap), (c) wing B (sinusoidal leading-edge wing without flap), and (d) wing B₁ (sinusoidal leading-edge wing with smart flap).

Table 1. Geometric properties of tested wings.

Wing	Leading-edge type	Flap type	Chord (cm)	Span (cm)	wavelength	Amplitude
A	Smooth	–	10	29	–	–
B	Sinusoidal	–	10	29	0.5 c	0.12 c
A ₁	Smooth	Smart	10	29	–	–
B ₁	Sinusoidal	Smart	10	29	0.5 c	0.12 c

with the freestream velocity. Furthermore, the starting point of the smart flap is 70% of the chord from leading-edge.

Wind tunnel and measurement instruments

The experiments are performed in an open circuit, low speed, and closed test section wind tunnel with a test section of 120 cm × 100 cm. Tests are carried out across different speeds of 5 m/s, 7 m/s, and 10 m/s. Reynolds number based on these freestream velocities and mean chord length are equal to 29,000, 40,000 and 58,000. Measurements are taken for each

wing for the angles of attack over the range of $0^\circ < \alpha < 36^\circ$. The turbulence intensity of the wind tunnel is 0.3% at a velocity of 5 m/s. This value for turbulence intensity is much less than that mentioned by Mueller.⁵²

Two one-dimensional strain gauge load cells (model Bongshin OBU-N49106 and OBU-N50170) are used to measure the lift and drag forces. The relative error of these force sensors is below 0.4%. The hysteresis, non-repeatability, and non-linearity of force sensors are less than 0.02% of full scale (3 kg and 6 kg).^{53,54} The relative uncertainty in force coefficients was determined to be less than 1%.

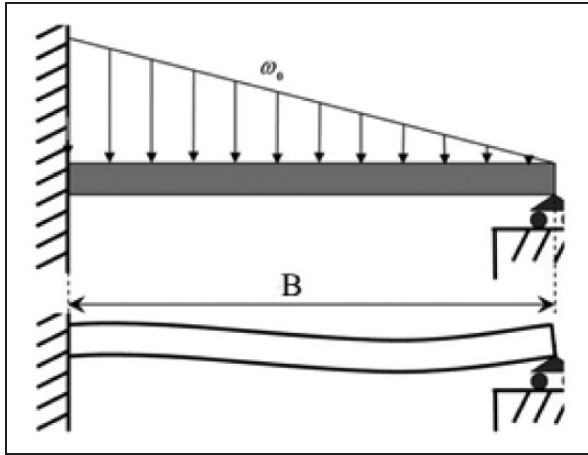


Figure 3. Schematic view of beam model.⁴²

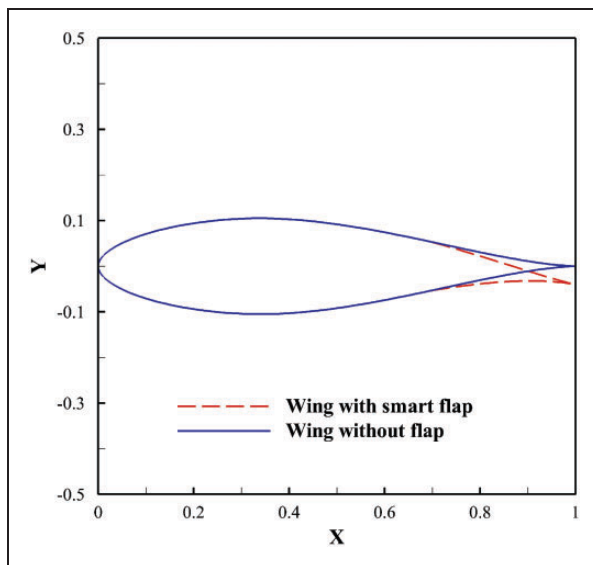


Figure 4. Difference between wing with smart flap and without flap.

As shown in Figure 5, the load cells are connected to a stepper motor (model ZhengKe motor ZGA42FH) and a stand at the top of the wind tunnel. As demonstrated, load cells are located in the right position. The mechanism for adjusting the angle of attack is shown in Figure 6. In this mechanism, the stepper motor (Figure 6(a)) is exploited to convert the rotational motion of the electrical motor to the wings via a radial roller bearing (Figure 6(b)). These components are assembled and then placed into a shield which is shown in Figure 6(c). Forces are acquired for 50 seconds for each case at 1000 Hz. Known weights are utilized to calibrate the load cells and the output functions are used to convert the average measured signals to force. The measured voltage by the load cell will be amplified by using an amplifier (model Dacell DN-AM100). A data acquisition board (model Advantech PCI-1710HG) is used to acquire all the signals. The model inside the wind tunnel is depicted in Figure 7.

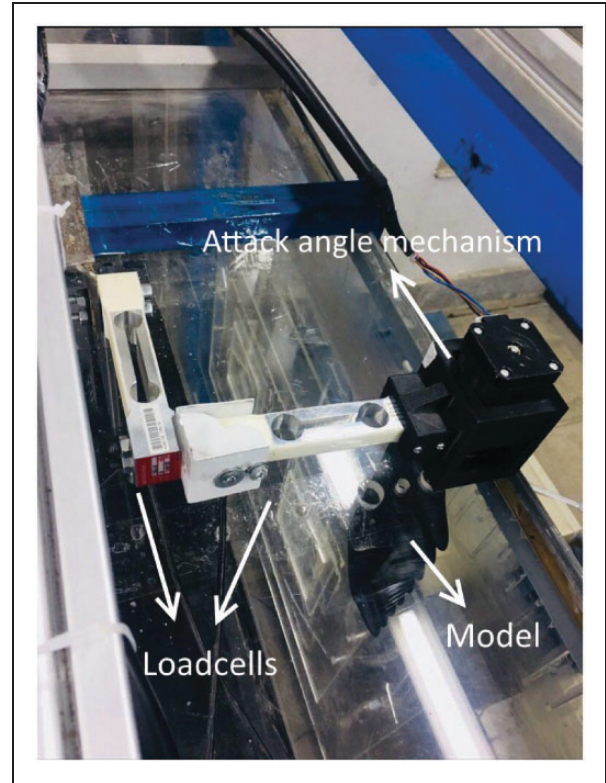


Figure 5. Designed and manufactured setups for load cells and attack angle adjustment.

It should be noted that in this experiment, in the worst case (lowest Reynolds number), about 2.95% of the wing is in the wind tunnel boundary layer. This content is less than that of Custodio et al.⁵¹ where the wind tunnel boundary layer covers 4.3 and 7.8% of the model span for the largest and smallest freestream velocities, respectively.

Validation

Lift and drag coefficients of the wing with sinusoidal leading-edge (wing B) at Reynolds number of 90,000 are compared to those of Custodio et al.⁵¹ and represented in Figure 8. As shown, there would be an acceptable agreement between outcomes of present experimental work and those of Custodio et al.⁵¹ The average error between lift and drag coefficients of the present study and data of Custodio et al.⁵¹ is 3.7% and 3.9%, respectively.

Results and discussion

Results obtained from experiments are divided into lift coefficient, drag coefficient, and lift to drag ratio sections. In each section, results for four manufactured wings are reported, justified, and compared with each other to indicate how smart flaps can change the aerodynamics of sinusoidal and smooth leading-edge wings. Furthermore, the effects of Reynolds number are analyzed in detail.

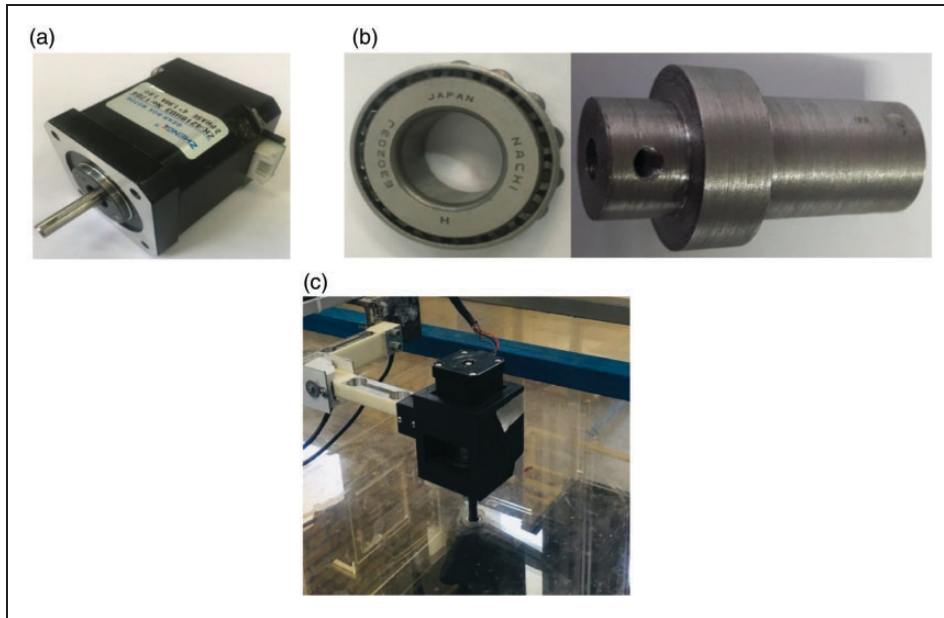


Figure 6. Views of the angle of attack mechanism: (a) stepper motor, (b) radial roller bearing, and (c) shield.

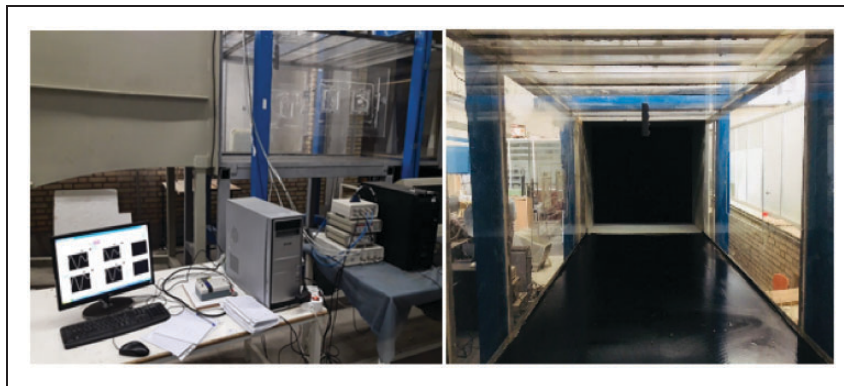


Figure 7. View of model inside the wind tunnel.

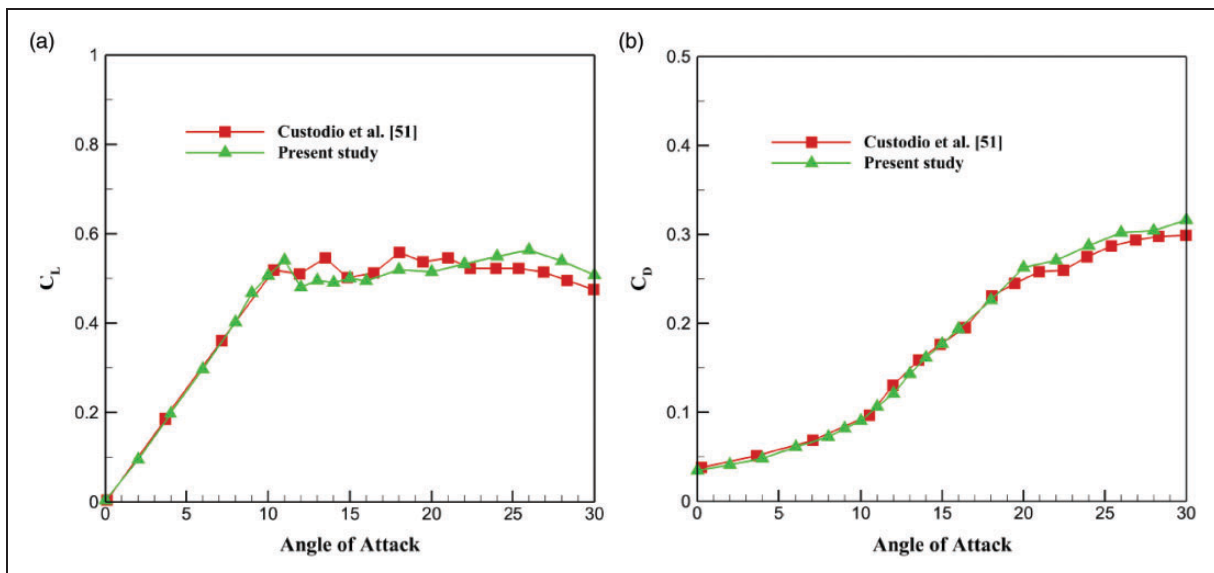


Figure 8. Comparison between aerodynamic coefficients of this study and those of Custodio et al.⁵¹ (a) Lift coefficient and (b) drag coefficient versus angle of attack.

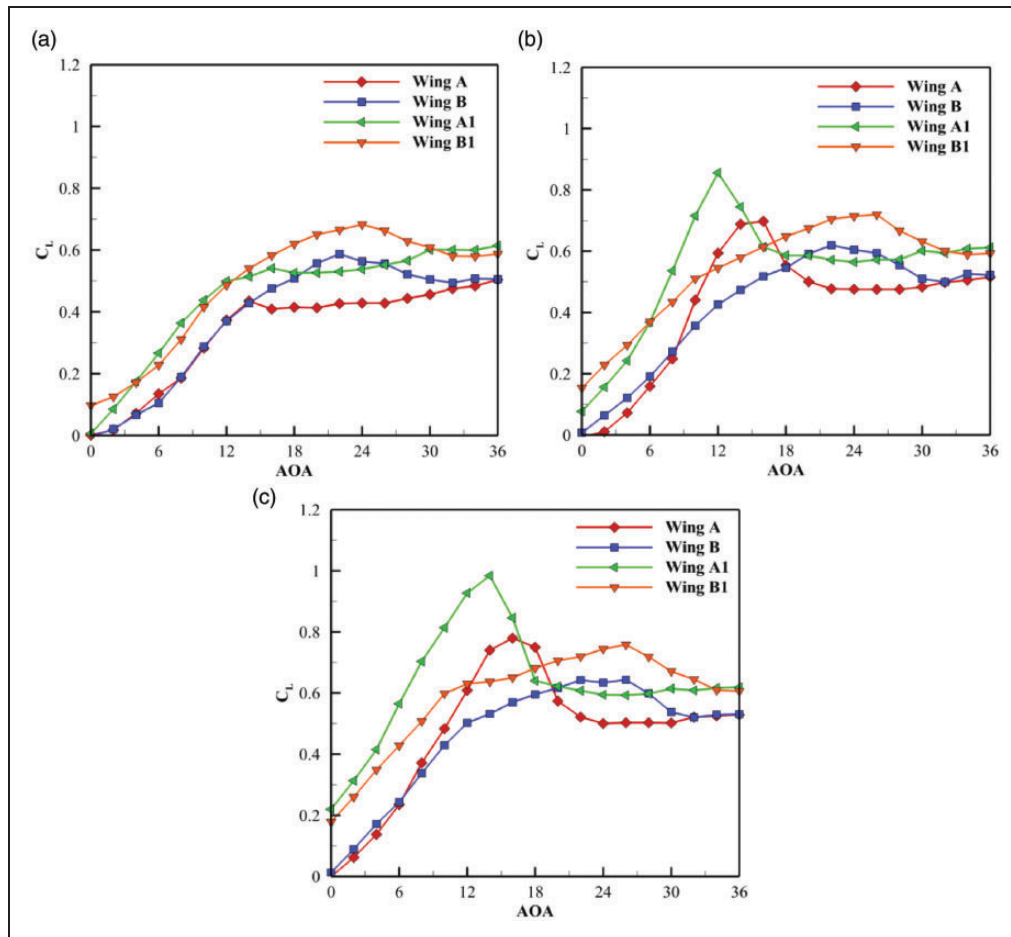


Figure 9. Variations of lift coefficient versus angle of attack; (a) $Re = 29,000$ (b) $Re = 40,000$, and (c) $Re = 58,000$.

Lift coefficient

The lift coefficient (C_L) versus the angle of attack is demonstrated in Figure 9 for four wings based on different Reynolds numbers. In $Re = 40,000$ the lift coefficient for wing A reaches a peak of about 0.70 at $\alpha = 16^\circ$. As many previous researchers showed,^{55,56} in low angles of attack, the flow is attached to the wing surface, resulting in a strong negative pressure region near the leading-edge. Therefore, the lift coefficient increases. However, in high angles of attack, laminar flow passing the upper surface of the wing faces an adverse pressure gradient. Subsequently, flow is separated as a shear layer since the laminar boundary layer has inherently lower kinetic energy. Once this shear layer is combined with the momentum of freestream, it reattaches to the wing surface as a turbulent boundary layer close to trailing-edge and creates laminar separation bubbles. It should be noted that the reattachment point moves toward trailing-edge and creates larger separation bubbles as the angle of attack increases. Further increment of the angle of attack causes the flow to be fully separated, resulting in a large reduction of lift coefficient.⁵⁷ Guerreiro and Sousa²⁶ expressed that bursting separation bubbles formed just

before stall is the main reason for sudden lift reduction after stall.

A maximum lift coefficient of 0.62 is obtained for wing B at $\alpha = 22^\circ$. Although, wing A averagely produces 28% higher lift coefficient than wing B for $8^\circ < \alpha < 18^\circ$, similar to Guerreiro and Sousa,²⁶ lift coefficient of wing B is 15% higher than that of wing A after stall ($18^\circ < \alpha < 32^\circ$) and also for $0^\circ < \alpha < 8^\circ$. On the other hand, the stall point is advanced to $\alpha = 12^\circ$ when the smart flap is added to the smooth leading-edge wing (wing A₁). Furthermore, C_{Lmax} significantly increases to 0.86 and the value of C_L is almost entirely higher than wing A. It should be noted that for $\alpha > 28^\circ$, the C_L of wing A₁ dominates the lift coefficient of wing B. This is because that the difference between pressure distribution of upper and lower surfaces of the wings with smart flap is higher than those without flap.⁴² Moreover, lift coefficient of wing B₁ is significantly higher than wing B. It should be noted that the C_L of wing B₁ reaches a peak of 0.72 at $\alpha = 26^\circ$, which is considerably higher than wing A. That is to say, adding smart flap to wing B increases the maximum lift coefficient while delays the stall point.

This finding is of importance since it proves that the combination of sinusoidal leading-edge wing with

trailing-edge smart flap can considerably enhance the aerodynamic performance while delays the stall angle. This is truly a good clue for engineers who tend to construct more maneuverable and agile aerial vehicles. Generally, it can be concluded that flaps increase the value of the lift coefficient for both sinusoidal and smooth leading-edge wings. However, they delay stall point for sinusoidal wing while stall is advanced when flaps are added to smooth wings. It is worth mentioning that the lift curve slope of sinusoidal leading-edge wings in all cases is less than that of smooth leading-edge ones.

In the lowest Reynolds number, the peak value observed in $Re = 40,000$ for wings A and A_1 disappears. As Yasuda et al.²⁷ explained, this is because even at low angles of attack, flow separation happens near the trailing-edge of these wings where the laminar vortices develop. The separation point moves toward leading-edge as the angle of attack further increases. In contrast to higher Reynolds number that separation bubbles are reattached to the wing surface, shear layer in the lowest Reynolds number is not able to reattach to the wing surface as a turbulent boundary layer, resulting in higher pressure drag and poor lift generation.⁵⁷ Therefore, a high discrepancy is observed between lift coefficients of these two Reynolds numbers. However, this difference becomes smaller in high angles of attack because flow separation is developed for both Reynolds numbers. As a result, the difference in pressure distribution becomes less than that of low angles of attack. At $Re = 29,000$, sinusoidal leading-edge in wings B and B_1 causes the flow to be attached by producing longitudinal vortices. Therefore, separation at upper surface of leading-edge imposes a negative pressure distribution at troughs.²⁷ Consequently, these two wings have a higher lift coefficient than wing A after the stall region. Indeed, when the fluid flow reaches sinusoidal leading-edge wings deflects toward the troughs and is separated. Separation bubbles in these zones create a strong negative pressure and subsequently spanwise pressure gradient. This spanwise pressure gradient, in turn, causes the flow to be moved from peaks toward troughs. Therefore, momentum is transferred to the separation region close to troughs and leads to flow reattachment.²⁷

For the highest Reynolds number, superiority of wing B in comparison with wing A emerges in the poststall region where sinusoidal leading-edge reinforces the flow reattachment particularly in troughs by producing longitudinal vortices while the flow is separated in wing A. However, due to reattachment of flow in higher Reynolds numbers of 40,000 and 58,000 over the wing A, the superiority of wing A is concluded compared to wing B before stall point. As indicated, flow over the first three-quarters of smooth leading-edge wings is attached in the prestall region while flow over half of the sinusoidal leading-edge wings is separated. This flow separation over

sinusoidal leading-edge wings happens due to the blunter leading-edge radius of curvature of troughs between adjacent protuberances. This difference causes a smooth leading-edge wing (wing A) to have a higher lift before stall than sinusoidal leading-edge wing (wing B). However, after stall, flow is fully separated over wing A while it is attached over leading-edge protuberances in wing B. After that, the almost same value is reported for both wings. On the other hand, the same behaviors as $Re = 40,000$ are reported for the wings with smart flaps at Reynolds number of 58,000 (wing A_1 and B_1). It should be noted that increasing the Reynolds number from 40,000 to 58,000 enhances the lift coefficient of all four wings. However, wing A_1 with a 17% increase in lift coefficient is the most affected wing while the lift coefficient of wing B increases by only 5%.

Drag coefficient

The drag coefficient (C_D) of all wings is illustrated in Figure 10 for different Reynolds numbers. It can be seen that all wings almost have the same drag coefficient for $\alpha < 6^\circ$. After that, the largest C_D values belong to the wings with smart flaps (wing A_1 and B_1). Strong flap tip vortex is formed for wing A_1 and B_1 which induces a great deal of downwash velocity on the wing, particularly in the flap region. Consequently, larger induced drag is produced for the wings with flap. Similarly to Johari et al.,¹³ wing A produces slightly less drag coefficient than wing B in the poststall regime. However, this is in contrast to what Yasuda et al.²⁷ claimed. They showed that the drag coefficient of sinusoidal leading-edge wings is almost the same as smooth leading-edge ones.

In contrast to lift coefficient diagrams, the drag coefficient is almost unchanged with Reynolds number for all wings. It should be noted that the slope of C_D diagrams for wings A and A_1 dramatically increases for $15^\circ < \alpha < 18^\circ$ at $Re = 40,000$ and 58,000 because of the stall. Next, the slope of the drag coefficient curve for these wings reduces but it is still higher than that reported for $\alpha < 6^\circ$.

Lift to drag ratio

Aerodynamic performance of wings, which is defined as the lift to drag ratio, versus angle of attack is shown in Figure 11 for four tested wings at different Reynolds numbers. As shown in Figure 11(b) for $Re = 40,000$, it is apparent that wing A_1 has higher aerodynamic performance than the wing A for $\alpha < 18^\circ$, while its stall point is advanced compared to wing A. Furthermore, maximum aerodynamic performance is obtained by wing A_1 . However, for $\alpha > 18^\circ$, almost the same lift to drag ratios for these two wings are reported. Furthermore, the capability of wing B_1 in producing higher lift to drag ratio than wing B is concluded for $\alpha < 12^\circ$. However, the

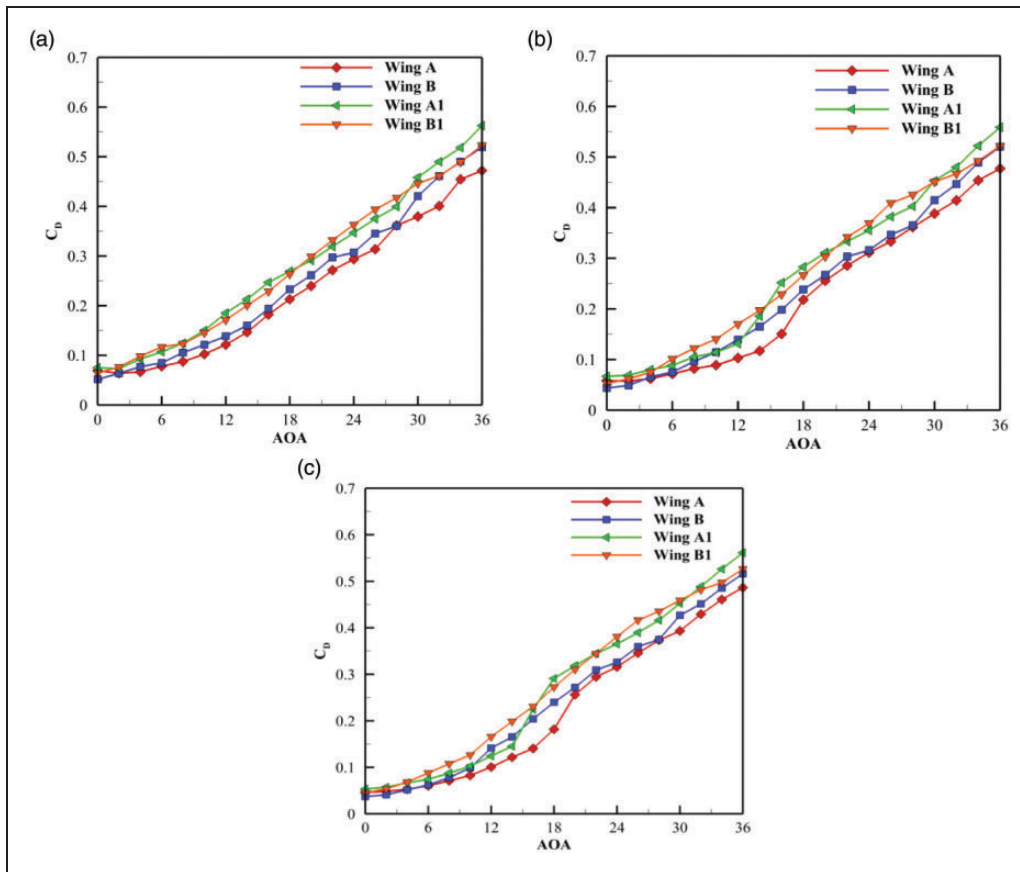


Figure 10. Variations of drag coefficient versus angle of attack; (a) $Re = 29,000$ (b) $Re = 40,000$, and (c) $Re = 58,000$.

aerodynamic performance of these two wings is almost identical after this angle. It should be reminded that as shown in the previous section, wings with smart flaps (A_1 and B_1) have more drag coefficients than those without flaps. Nevertheless, the excellent performance of wings with smart flaps in producing a higher lift coefficient causes them to have a higher lift to drag ratio compared to wings without flaps. It can be deduced that sinusoidal leading-edge wings (wing B and B_1) have higher performance than smooth leading-edge wings (wing A and A_1) in the poststall regime, although this difference is slight.

The effects of Reynolds number on the aerodynamic performance of manufactured wings are depicted in Figure 11. It is shown that the difference among lift to drag ratios of the wings is the smallest for the lowest Reynolds number. However, as Reynolds number increases, the discrepancy among lift to drag ratio increases for $\alpha < 18^\circ$. It should be noted that aerodynamic performance of all wings enhances with Reynolds number, and the greatest improvement belongs to the smooth leading-edge wing without flap, whereas sinusoidal leading-edge wing with smart flap is the least affected wing. Furthermore, wings with smart flap bring obvious benefits compared to the same wings without flap in all Reynolds numbers. However, the effect of the

smart flap on the smooth leading-edge wing is more than that with sinusoidal leading-edge. Therefore, it can be considered as a positive point by engineers who tend to build bio-inspired wings with the highest performance.

The main aerodynamic characteristics including, lift curve slope, maximum C_L , angle of maximum C_L , minimum C_D , maximum C_L/C_D , and angle of maximum C_L/C_D for tested wings have been tabulated in Table 2. The slope of the lift curve, $dC_L/d\alpha$, is computed before the stall angle for each wing. Similarly to Johari et al.,¹³ lift curve slope of wing A is higher than that of wing B. Furthermore, using smart flap at trailing-edge of smooth leading-edge wing causes lift curve slope to be increased by 30% while smart flap declines the lift curve slope of the sinusoidal leading-edge wing by 25%. According to this table, the maximum lift coefficient of wing A_1 and B_1 is 23% and 16% higher than that of wing A and B, respectively. As expressed before, wing A_1 advances the stall point by 4 degrees compared to wing A, while the stall point of wing B_1 is 4 degree higher than that of wing B. Adding smart flaps to smooth and sinusoidal leading-edge wings increase the minimum drag coefficient by 15% and 21%, respectively, which can be considered as a disadvantage of smart flaps. However, the maximum lift to drag ratio for wing A goes up by 11% when smart flaps are added at

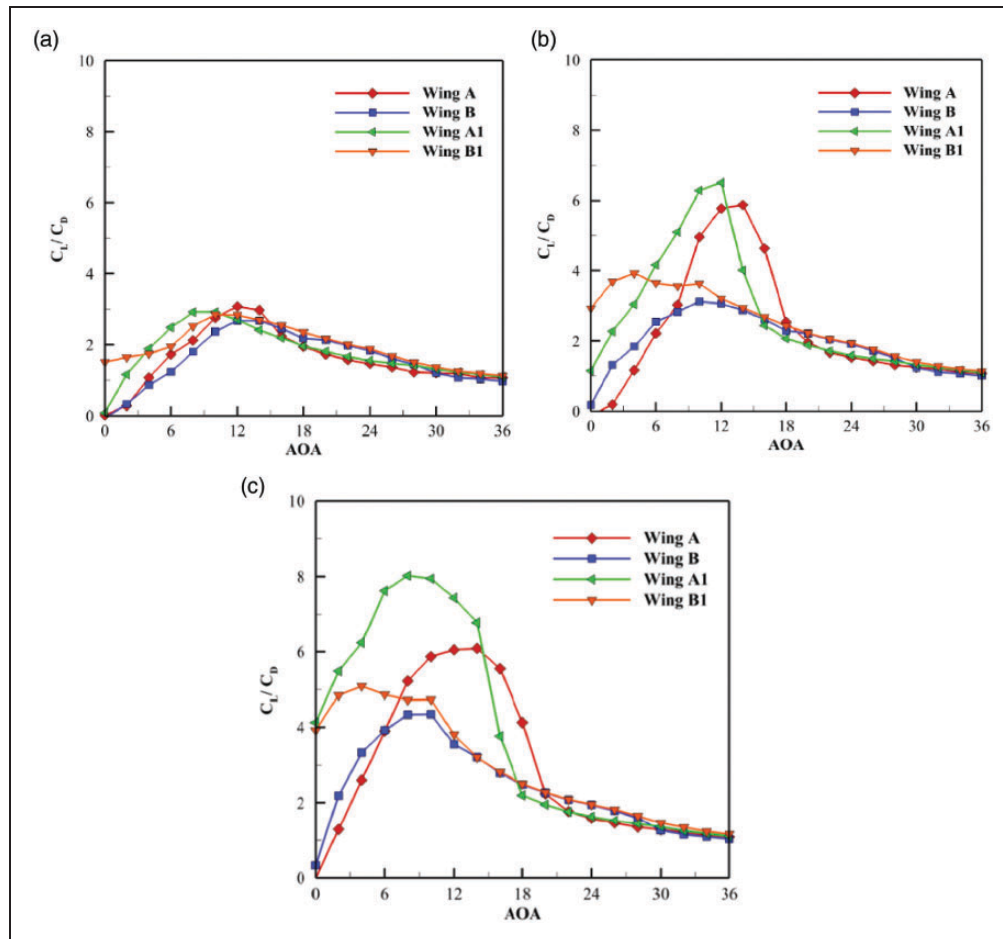


Figure 11. Variations of lift to drag ratio versus angle of attack; (a) $Re = 29,000$, (b) $Re = 40,000$, and (c) $Re = 58,000$.

Table 2. Aerodynamic characteristics of four wings at $Re = 40,000$.

Wing	$dC_L/d\alpha$ (per deg)	C_{Lmax}	α at C_{Lmax} (deg)	C_{Dmin}	$(C_L/C_D)_{max}$	α at $(C_L/C_D)_{max}$ (deg)
A	0.0514	0.6977	16	0.0580	5.8731	14
A ₁	0.0670	0.8561	12	0.0668	6.5111	12
B	0.0293	0.6197	22	0.0436	3.1228	10
B ₁	0.0219	0.7195	26	0.0526	3.9229	4

the trailing-edge. This amount for wing B is 25% which is significantly higher than that of wing A. That is to say, although sinusoidal leading-edge wings with and without flaps have an entirely less maximum lift to drag ratio compared to wing A and A₁, effects of smart flaps on the sinusoidal leading-edge wing are more obvious from lift to drag ratio point of view. It is worth mentioning that the enhancement in the lift to drag ratio is obtained at a smaller angle of attack for both wing A₁ and B₁ compared to wing A and B, respectively.

Conclusion

The goal of this research study was to analyze the effects of smart flaps on the aerodynamics of sinusoidal and smooth leading-edge wings. Hence, four

wings with different leading-edge configurations (smooth and sinusoidal), and different trailing-edge shapes (no flap and smart flap) were constructed. Wind tunnel tests were conducted to compare these four wings for a wide range of angles of attack and different low Reynolds numbers. It was found that smart flap in smooth leading-edge wing advances the stall point while it delays the stall for the sinusoidal leading-edge wing, and the maximum lift coefficient significantly enhances for both smooth and sinusoidal leading-edge wings with smart flap. Furthermore, it was indicated that using smart flap causes both wings to have a higher lift coefficient compared to those without flap based on all Reynolds numbers. Generally, it can be concluded that the effects of the sinusoidal leading-edge wing, which is primarily used to delay the stall and produce

higher lift force after stall point, are enhanced by employing smart flap. This finding would be of high importance for the vehicles that require high maneuverability.

Declaration of Conflicting Interests

The author(s) declared no potential conflicts of interest with respect to the research, authorship, and/or publication of this article.

Funding

The author(s) received no financial support for the research, authorship, and/or publication of this article.

ORCID iDs

MH Djavareshkian  <https://orcid.org/0000-0003-1766-1190>

B Forouzi Feshalami  <https://orcid.org/0000-0002-4457-3674>

References

1. Van Nierop EA, Alben S and Brenner MP. How bumps on whale flippers delay stall: an aerodynamic model. *Phys Rev Lett* 2008; 100: 054502.
2. Hassanalain M, Salazar R and Abdelkefi A. Conceptual design and optimization of a tilt-rotor micro air vehicle. *Chin J Aeronaut* 2019; 32: 369–381.
3. Goruney T and Rockwell D. Flow past a Delta wing with a sinusoidal leading edge: near-surface topology and flow structure. *Exp Fluids* 2009; 47: 321–331.
4. Sudhakar S, Karthikeyan N and Venkatakrishnan L. Influence of leading edge tubercles on aerodynamic characteristics of a high aspect-ratio UAV. *Aerosp Sci Technol* 2017; 69: 281–289.
5. Malipeddi AK, Mahmoudnejad N and Hoffmann KA. Numerical analysis of effects of leading-edge protuberances on aircraft wing performance. *J Aircr* 2012; 49: 1336–1344.
6. Ozen CA and Rockwell D. Control of vortical structures on a flapping wing via a sinusoidal leading-edge. *Phys Fluids* 2010; 22: 021701.
7. Wang Z and Zhuang M. Leading-edge serrations for performance improvement on a vertical-axis wind turbine at low tip-speed-ratios. *Appl Energy* 2017; 208: 1184–1197.
8. Kumar VV and Shah DA. Application of tubercles in wind turbine blades: a review. *Appl Mech Mater* 2017; 867: 254–260.
9. Huang G-Y, Shiah YC, Bai C-J, et al. Experimental study of the protuberance effect on the blade performance of a small horizontal axis wind turbine. *J Wind Eng Ind Aerodyn* 2015; 147: 202–211.
10. Custodio D, Henoch C and Johari H. Cavitation on hydrofoils with leading edge protuberances. *Ocean Eng* 2018; 162: 196–208.
11. Wei Z, New TH and Cui YD. An experimental study on flow separation control of hydrofoils with leading-edge tubercles at low Reynolds number. *Ocean Eng* 2015; 108: 336–349.
12. Keerthi MC, Rajeshwaran MS, Kushari A, et al. Effect of leading-edge tubercles on compressor cascade performance. *AIAA J* 2016; 54: 912–923.
13. Johari H, Henoch CW, Custodio D, et al. Effects of leading-edge protuberances on airfoil performance. *AIAA J* 2007; 45: 2634–2642.
14. Zverkov I, Zanin B and Kozlov V. Disturbances growth in boundary layers on classical and wavy surface wings. *AIAA J* 2008; 46: 3149–3158.
15. Hansen KL, Kelso RM and Dally BB. Performance variations of leading-edge tubercles for distinct airfoil profiles. *AIAA J* 2011; 49: 185–194.
16. Dropkin A, Custodio D, Henoch CW, et al. Computation of flow field around an airfoil with leading-edge protuberances. *J Aircr* 2012; 49: 1345–1355.
17. Zhang MM, Wang GF and Xu JZ. Aerodynamic control of low-Reynolds-number airfoil with leading-edge protuberances. *AIAA J* 2013; 51: 1960–1971.
18. Cai C, Zuo Z, Maeda T, et al. Periodic and aperiodic flow patterns around an airfoil with leading-edge protuberances. *Phys Fluids* 2017; 29: 115110.
19. Cai C, Zuo Z, Liu S, et al. Effect of a single leading-edge protuberance on NACA 634-021 airfoil performance. *J Fluids Eng* 2018; 140: 021108.
20. Bolzon MD, Kelso RM and Arjomandi M. Performance effects of a single tubercle terminating at a swept wing's tip. *Exp Therm Fluid Sci* 2017; 85: 52–68.
21. Bolzon MD, Kelso RM and Arjomandi M. Force measurements and wake surveys of a swept tubercled wing. *J Aerosp Eng* 2017; 30: 04016085.
22. Aftab SMA and Ahmad KA. CFD study on NACA 4415 airfoil implementing spherical and sinusoidal tubercle leading edge. *PLoS One* 2017; 12: e0183456.
23. Lin S-Y, Lin Y-Y, Bai C-J, et al. Performance analysis of vertical-axis-wind-turbine blade with modified trailing edge through computational fluid dynamics. *Renew Energy* 2016; 99: 654–662.
24. Prigent SL, Buxton ORH and Bruce P. Wake of a lifting wing with cut-in sinusoidal trailing edges. *AIAA J* 2017; 55: 1590–1601.
25. Rostamzadeh N, Kelso RM and Dally B. A numerical investigation into the effects of Reynolds number on the flow mechanism induced by a tubercled leading edge. *Theor Comput Fluid Dyn* 2017; 31: 1–32.
26. Guerreiro JLE and Sousa J. Low-Reynolds-number effects in passive stall control using sinusoidal leading edges. *AIAA J* 2012; 50: 461–469.
27. Yasuda T, Fukui K, Matsuo K, et al. Effect of the Reynolds number on the performance of a NACA0012 wing with leading edge protuberance at low Reynolds numbers. *Flow Turbul Combust* 2019; 102: 435–455.
28. Esmaeili A, Delgado HEC and Sousa J. Numerical simulations of low-Reynolds-number flow past finite wings with leading-edge protuberances. *J Aircr* 2018; 55: 226–238.
29. Papadopoulos C, Katsiadramis V and Yakinthos K. Influence of tubercles' spanwise distribution on swept wings for unmanned aerial vehicles. *Proc IMechE, Part G: J Aerospace Engineering* 2020; 00954410020919583.
30. Sreejith BK and Sathyabhama A. Experimental and numerical study of laminar separation bubble

- formation on low Reynolds number airfoil with leading-edge tubercles. *J Braz Soc Mech Sci Eng* 2020; 42: 171.
31. Bolzon MD, Kelso RM and Arjomandi M. Tubercles and their applications. *J Aerosp Eng* 2016; 29: 04015013.
 32. Aftab SMA, Razak NA, Mohd Rafie AS, et al. Mimicking the humpback whale: an aerodynamic perspective. *Prog Aerosp Sci* 2016; 84: 48–69.
 33. Forster E, Sanders B and Eastep F. Modelling and sensitivity analysis of a variable geometry trailing edge control surface. In: *44th AIAA/ASME/ASCE/AHS/ASC Structures, Structural Dynamics, and Materials Conference*, Norfolk, VA, 2003.
 34. Bolonkin A and Gilyard GB. Estimated benefits of variable-geometry wing camber control for transport aircraft. *NASA/TM-1999-206586*, 1999.
 35. Pern N and Jacob J. Wake vortex mitigation using adaptive airfoils – the piezoelectric arc airfoil. In: *37th Aerospace Sciences Meeting and Exhibit*, Reno, NV, USA, 1999.
 36. Abdullah E, Bil C and Watkins S. Application of smart materials for adaptive airfoil shape control. In: *47th AIAA Aerospace Sciences Meeting including The New Horizons Forum and Aerospace Exposition*, Orlando, Florida, 2009.
 37. Tiseo B, Koopmann G, Concilio A, et al. Smart tuneable dynamic vibration absorbers. In: *12th AIAA/CEAS Aeroacoustics Conference (27th AIAA Aeroacoustics Conference)*, Cambridge, Massachusetts, 2006.
 38. Djavarehshkian MH and Esmaeli A. Application of smart flap for race car wings. *Int J Aerodyn* 2012; 2: 66–92.
 39. Barlas TK and van Kuik G. Review of state of the art in smart rotor control research for wind turbines. *Prog Aerosp Sci* 2010; 46: 1–27.
 40. Cinquemani S, Diana G, Fossati L, et al. A smart structure for wind tunnel investigation of a bridge deck's vortex-induced torsional motion. *Mechatronics* 2016; 33: 108–120.
 41. Chinnassamy P and Chen Y. Application of computational fluid dynamics on smart wing design. In: *43rd AIAA Aerospace Sciences Meeting and Exhibit*, Reno, NV, 2005.
 42. Djavarehshkian MH, Esmaeli A and Parsani A. Aerodynamics of smart flap under ground effect. *Aerosp Sci Technol* 2011; 15: 642–652.
 43. Djavarehshkian MH, Esmaeli A and Parsania A. Numerical simulation of smart hydrofoil in marine system. *Ocean Eng* 2013; 73: 16–24.
 44. Lee T and Gerontakos P. Dynamic stall flow control via a trailing-edge flap. *AIAA J* 2006; 44: 469–480.
 45. Lackner MA and van Kuik G. A comparison of smart rotor control approaches using trailing edge flaps and individual pitch control. *Wind Energy* 2010; 13: 117–134.
 46. Liu T, Montefort J, Liou W, et al. Lift enhancement by static extended trailing edge. *J Aircr* 2007; 44: 1939–1947.
 47. Hassanalian M and Abdelkefi A. Classifications, applications, and design challenges of drones: a review. *Prog Aerosp Sci* 2017; 91: 99–131.
 48. Sepahi-Younsi J, Forouzi Feshalami B, Maadi SR, et al. Boundary layer suction for high-speed air intakes: a review. *Proc IMechE, Part G: J Aerospace Engineering* 2019; 233: 3459–3481.
 49. Samiee A, Djavarehshkian MH, Forouzi Feshalami B, et al. Improvement of airfoils aerodynamic efficiency by thermal camber phenomenon at low Reynolds number. *J Aerosp Technol Manag* 2018; 10.
 50. Lohry MW, Clifton D and Martinelli L. Characterization and design of tubercle leading-edge wings. In: *Seventh International Conference on Computational Fluid Dynamics (ICCFD7)*, Big Island, Hawaii, 2012, pp. 9–13.
 51. Custodio D, Henoch CW and Johari H. Aerodynamic characteristics of finite span wings with leading-edge protuberances. *AIAA J* 2015; 53: 1878–1893.
 52. Mueller TJ. *Aerodynamic measurements at low Reynolds numbers for fixed wing micro-air vehicles*. Notre Dame University, Department of Aerospace and Mechanical Engineering, 2000.
 53. Forouzi Feshalami B, Djavarehshkian MH, Zaree AH, et al. The role of wing bending deflection in the aerodynamics of flapping micro aerial vehicles in hovering flight. *Proc IMechE, Part G: J Aerospace Engineering* 2019; 233: 3749–3761.
 54. Forouzi Feshalami B, Djavarehshkian M, Yousefi M, et al. Experimental investigation of flapping mechanism of the black-headed gull in forward flight. *Proc IMechE, Part G: J Aerospace Engineering* 2019; 233: 4333–4349.
 55. Hansen KL, Rostamzadeh N, Kelso RM, et al. Evolution of the streamwise vortices generated between leading edge tubercles. *J Fluid Mech* 2016; 788: 730–766.
 56. Rostamzadeh N, Hansen KL, Kelso RM, et al. The formation mechanism and impact of streamwise vortices on NACA 0021 airfoil's performance with undulating leading edge modification. *Phys Fluids* 2014; 26: 107101.
 57. Winslow J, Otsuka H, Govindarajan B, et al. Basic understanding of airfoil characteristics at low Reynolds numbers (104–105). *J Aircr* 2018; 55: 1050–1061.